Carbon Nanotube Functionalization and Scaffold Topography Guide Differentiation of Myoblasts

by

Akhil Patel

Bachelor of Pharmacy, Gujarat Technological University, 2012.

Submitted to the Graduate Faculty of

School of Pharmacy in partial fulfillment

of the requirements for the degree of

Master of Science

University of Pittsburgh

2015

UNIVERSITY OF PITTSBURGH

School of Pharmacy

This thesis was presented

by

Akhil Patel

It was defended on

July 23, 2015

and approved by

Dr. Shilpa Sant, Assistant Professor, School of Pharmacy

Dr. Xiaochao Ma, Associate Professor, School of Pharmacy

Dr. Vinayak Sant, Assistant Professor, School of Pharmacy

Thesis Director Advisor: Dr. Shilpa Sant, Assistant Professor, School of Pharmacy

Carbon Nanotube Functionalization and Scaffold Topography Guide Differentiation of Myoblasts

Akhil Patel, B. Pharm

University of Pittsburgh, 2015

Recreating native microenvironment and providing appropriate guidance cues are instrumental in the design of regenerative scaffolds. Despite decades of research in skeletal muscle tissue engineering, there is limited clinical success in developing such regenerative scaffolds. This may be attributed to limited success in building complex features of native skeletal muscle tissue in synthetic scaffolds. These complex features include electroactivity of skeletal muscle cells, nano- (myofibrils) to macro-scale (muscle fiber bundles) hierarchical architecture along with aligned fibrous structure to provide contact guidance. Although scaffolds possessing each of these features have been built, combining multiple such features into a single scaffold still remains a challenge. Electrically conductive carbon-based scaffolds can be processed to possess multi-scale hierarchy along with porous structure and different geometries making them a potential candidate for skeletal muscle tissue engineering. Carbon-based materials have been explored mostly for their application in energy storage and electronics; however, few studies have evaluated their applications in tissue engineering. In this study, we investigated potential of carbon-based scaffolds with different geometries (interconnected porous *vs* aligned fibrous structure) and nanoscale surface functionalization (carbon nanotube) for skeletal muscle tissue engineering. We engineered multiscale hierarchical scaffolds based on carbon materials, namely, highly porous carbon foams and highly aligned carbon fibers. Both porous foam scaffolds and aligned fibrous scaffolds were nano-functionalized with carbon nanotube (CNT) and silica-CNT (only foams) coatings on their surfaces. It was hypothesized that aligned fibrous structure and nanoscale CNT coatings will provide synergistic guidance cues to enhance myoblast

differentiation. Additionally, immobilization of CNTs on the scaffold surface will obviate the cytotoxicity issues. The results showed combined role of surface modification (CNT functionalization) and alignment cues to facilitate cell adhesion, growth and differentiation. Surface functionalization of porous carbon foams with CNT and silica-CNT provided physico-chemical cues for skeletal muscle cells to differentiate into myocytes; however, failed to promote their fusion into functional multinucleated myotubes. More interestingly, CNT nano-functionalization coupled with alignment cues in the form of aligned carbon fibers were able to overcome this limitation leading to formation of continuous multinucleated myotubes. In summary, CNT functionalization and aligned scaffold architecture improved cell-material interaction and promoted the process of myogenesis.

Keywords: Skeletal muscle, Tissue engineering, Carbon nanotubes, C2C12, Myogenesis.

TABLE OF CONTENTS

------------------------------------Intentionally left blank--

LIST OF FIGURES

ACKNOWLEDGEMENTS

I would like to thank University of Pittsburgh, School of Pharmacy, for giving me the opportunity to study here. I sincerely thank my advisor Dr. Shilpa Sant for guiding me through my studies. I would like to thank Dr. Vinayak Sant, Dr. Maggie Folan and other faculty members in School of Pharmacy for their constant support and guidance. I would like to thank our collaborator, Dr. Sharmila Mukhopadhyay and graduate students in her lab, namely Wenhu Wang and Anil Karumuri for providing me with the carbon materials which I used in this research. I sincerely thank Dr. Robert Gibbs for access to confocal microscope. I would like to thank Dr. Donna Stolz for access to scanning electron microscopy. I would like to thank Lori Schmotzer for all the administrative help throughout my studies.

I would like to thank my friends and colleagues in the lab Dr. Manjulata Singh, Dr. Kishor Sarkar, Yingfei Xue, Chen Yuzhe, Shilpaa Mukundan, Harini Krishnan, Jean Jr. Liu, Piyusha Sane, Tatyana Yatsenko and Dr. Maria Jaramillo for their help.

My sincere thanks to all the faculty, staff and fellow graduate students from the School of Pharmacy.

I am immensely thankful to my parents, grandparents, my brother Jignesh and late uncle Chandrakant Patel for their constant encouragement and for teaching me values and the art of living.

1.0 INTRODUCTION

Skeletal muscle injuries account for about 55% of the total injuries sustained in sports. Every year, about 100,000 cases of muscle injuries are reported (US Bureau of Labor statistics, 2011). Similarly, injuries due to trauma and tumor ablation procedures result in skeletal muscle damage. Due to limited regenerative potential of the muscle, therapeutic strategies aimed at functional muscle regeneration are gaining importance. Some of the strategies used in the past such as transplant of autologous muscle and injection of satellite cells have shown limited success due to donor site morbidity, poor integration and survival of implanted tissue or cells [1, 2]. These problems can be circumvented by use of cell-interactive, and preferably, biodegradable ECM-mimicking materials to promote effective regeneration of skeletal muscle. Cell-ECM interactions can further facilitate essential cellular processes for normal muscle growth and development, including its regeneration [3, 4]. Hence, recent tissue engineering strategies are aimed at creating novel synthetic extracellular matrix (ECM)-mimics that recapitulate the structural and topographical cues present in native ECM [4-7]. Several approaches have been developed to create synthetic ECM-mimics such as nanofibrous electrospun scaffolds and hydrogels to enhance cell proliferation and differentiation [8-10]. However, matching intricate structure and complexity of the native muscle environment with synthetic materials still remains a daunting challenge [11]. Nonetheless, through basic research on skeletal muscle development, injury and regeneration, it is widely recognized that a combination of biochemical and

biophysical stimuli is critical for guiding the progenitor cells to appropriate orientation in order to promote uniformly aligned and well-organized muscle bundles [12]. Thus, efforts are directed to design materials with structural and/or biophysical cues in order to recreate the microenvironment conducive for myogenesis. Several of such materials with ECM-mimetic architectural and topographical cues for heart muscle tissue engineering have been reviewed by Parker *et al*. [13].

Native muscle structure exhibits multiscale hierarchy from myofibrils, to muscle fibers, which then bundle to form a functional muscle. Thus, it is desirable to have similar hierarchy in the scaffold. In addition, macroporous architecture of scaffold allows easy exchange of nutrients and waste products and it facilitates cell infiltration [14]. For example, honeycomb-like foam structures have been investigated for myocardial regeneration and peculiar interconnected honeycomb architecture was thought to reinforce the scaffold during the continuous contraction and relaxation process of myocardial tissue [15, 16]. In addition to scaffold architecture, adhesion of cells to the surface of the material is critical for skeletal muscle tissue engineering. Surface topography, especially nanoscale surface roughness can be an important feature in improving cell-scaffold interaction and cell adhesion. Similarly, surface wettability can affect cell adhesion on the scaffold surface. For example, moderately hydrophobic surfaces with contact angles around 70° facilitate better attachment of cells to scaffolds through strong binding of cellular adhesion proteins [17]. Skeletal muscle tissue is electrically excitable; hence electroactive materials may allow local delivery of electrical stimulus to enhance cell proliferation, differentiation and tissue damage. Indeed, conductive materials have shown to improve skeletal muscle cell (myoblast) differentiation into myocytes [18, 19]. It has been extremely challenging to engineer a scaffold with all these features. Thus, for functional skeletal muscle regeneration, it

is essential to build complex features such as electroactivity, nano-(myofibrils) to macro-scale (muscle fiber bundles) hierarchical architecture along with aligned fibrous structure to provide contact guidance. Although scaffolds possessing each of these features have been built, combining multiple such features into a single scaffold still remains a challenge. Electrically conductive carbon-based scaffolds can be processed to possess multi-scale hierarchy along with porous structure and different geometries making them a potential candidate for skeletal muscle tissue engineering.

Carbon-based materials have been used as conductive materials and also in energy storage-related applications [20-22]. They have been recently explored for various tissue engineering applications such as osteoblast growth [23], neural cell growth [24], as bone implants and drug delivery [25-27]. For example, Li *et al.* used 3D graphene foams to provide electrically conductive and macro-porous surface in order to promote proliferation and enhance differentiation of neural stem cells [28]. However, application of such foam structures in skeletal muscle tissue engineering remains to be tested. Their inert nature, processability into different sizes, shapes and architecture as well as their robust mechanical properties are some of the features that distinguish carbon-based scaffolds from other biomaterials for tissue engineering applications [23]. In this study, we introduce hierarchical carbon-based materials to investigate their potential in promoting skeletal muscle differentiation. They possess multi-scale hierarchy spanning from highly ordered nano-scale architecture to well-organized micro-scale architecture.

We engineered multiscale hierarchical scaffolds based on carbon materials, *viz.* carbon foams with highly interconnected porous structure [29] and carbon fibers with highly aligned fibrous structure. Surfaces of both porous foam and aligned fibrous scaffolds were further nano-functionalized with CNT and silica-CNT (Si-CNT) coatings to modulate their hydrophilic-

hydrophobic (wetting) properties and surface roughness. CNTs are an excellent nanomaterial of choice as they have been shown to promote myoblast differentiation [30, 31]. Along with electrical conductivity, they also impart the nano-surface roughness for the adhesion and spreading of cells. In our study, we specifically investigated effects of porosity and alignment of scaffolds (scaffold geometry), and nanostructure (CNT/Si-CNT) surface functionalization on myotube formation. It was hypothesized that aligned fibrous structure and nanoscale CNT coatings will provide synergistic guidance cues for myoblast differentiation into myotubes.

2.0 MATERIALS AND METHODS

2.1 Materials

Cell culture media, Dulbecco's phosphate buffered saline (DPBS) and serum were purchased from Mediatech Inc. (Manassas, USA). The cell culture supplies including media, serum were purchased from Mediatech® / Corning unless otherwise specified. The C2C12 cells were a kind gift from Dr. Feinberg at Carnegie Mellon University, USA.

2.2 Surface Coating of Carbon Foams and Fibers

Reticulated vitreous carbon (RVC) foams are typically fabricated from the pyrolysis of thermosetting polymer foam, resulting in skeleton or vitreous carbon struts. RVC foams selected in this study were with 80 pores per inch (PPI), provided by Ultramet Inc. Floating CNT carpets were synthesized using a two-step process previously developed by Mukhopadhyay group [32, 33]. Tetraethyl orthosilicate [TEOS; Si(OCH2CH3)4, Si-OEt (Alfaa aesar; 98%)] was used as a precursor. The first step involves deposition of silicon oxide (SiOx) activation/buffer layer via room temperature Microwave Plasma Enhanced Chemical Vapor Deposition (M-PECVD) reactor. The hexamethyldisiloxane [HMDSO, (CH3)6Si2O; sigma Aldrich, 99.5%] was used as a precursor in conjunction with 99.9% pure oxygen followed by CNT growth. This is followed by

chemical vapor deposition (CVD) of CNT using xylene (C8H10) and ferrocene [Fe(C5H5)2; Alfa Aesar, 99%] as a carbon and catalyst source, respectively. Silica coating was applied using methods described in our previously reported study [29]. Briefly, Acid catalyzed sol-gel process was utilized in order to produce the silica coating on the CNT-grafted hierarchical substrate. Entire fabrication was carried out by Mukhopadhyay group at Wright State University, USA. Plain weave carbon fiber mats were obtained from Hexcel (ACGP206-P). They were coated with CNTs as described above for the foams.

2.3 Measurement of Contact Angle

The contact angles of pristine and functionalized Foams and Fibers were investigated using the dynamic contact angle measurements designed in lab by Mukhopadhyay group. A drop of de-ionized water was added on the samples using a 21G needle and the image was captured after 10 s. The contact angle was measured using Solidworks.

2.4 Scanning Electron Microscopy (SEM)

Surface characterization of as prepared and cell-seeded Foam and Fiber scaffolds was carried out using SEM (JEOL 9335 Field Emission SEM). Cell-seeded scaffolds were fixed following 21 days and 14 days of culture for Foams and Fibers, respectively. SEM was performed following air drying for 24 h. Scaffolds were sputter-coated with 5 nm of gold-

palladium using Cressington 108 auto sputter coater. Images were obtained using accelerated voltage of 3 kV and a working distance of 8 mm.

2.5 C2C12 Mouse Myoblast Culture

The mouse myoblast cells (C2C12) cells were cultured in Dulbecco's modified Eagle's medium (DMEM) supplemented with 10% of heat inactivated Fetal Bovine Serum (Hyclone, Thermo Scientific) and 1% antibiotic (Penicillin and streptomycin). The cells were cultured in T75 flasks in a humidified incubator (37 ºC and 5% CO2), media was changed every 2 days and cells were passaged at confluence.

2.6 Cell Seeding on Foams and Fibers

The cylindrical foams of height 0.5 cm and diameter 0.5 cm were sterilized for 30 min in 70% isopropanol under UV. The foams were seeded with a seeding density of $2.54x10^6$ cells/cm^3. For metabolic activity assessment, the cells were seeded and cultured for 14 days in growth medium. For differentiation studies, the scaffolds were cultured in growth media till day 3 followed by differentiation media (DMEM supplemented with 10% heat inactivated horse serum, supplier). The samples were cultured for 21 days.

The fiber meshes of size 1cm x1cm were seeded with C2C12 cells of seeding density of $2.54x10^6$ cells/cm^3 as mentioned above. The study was carried out over a period of 14 days.

2.7 Metabolic Activity of Cells

The metabolic activity of cells seeded on Foams or Fibers were measured using the Alamar Blue assay (Nalgene, USA).The assay was performed over a period of 14 days. Alamar Blue solution (10% v/v) was prepared in complete growth media and 1 mL of this solution was added to each well containing cell-seeded scaffold and incubated for 4 h at 37 ºC. After this step, 100 µL of the solution from each well was added to 96-well plate and the fluorescence was read at 530 and 590 nm using the microplate reader (Corning Inc., USA). The wells containing only Alamar Blue solution in media was used for background fluorescence. Pristine carbon Foams and Fibers were used as control to compare the proliferation on functionalized Foams and Fibers.

2.8 Immunofluorescence Staining

Cell-seeded Foams or Fibers were fixed with 4% paraformaldehyde and washed 3 times with DPBS followed by the blocking/ permeabilization with DPBS containing 0.1% Triton X-100 and 5% BSA for 1 h at room temperature. The scaffolds were then incubated with the primary antibody against myosin heavy chain (MHC), MF-20 (1:50, DSHB, Iowa) overnight at 4 °C and washed with PBS three times. The scaffolds were then stained with secondary antibody (Alexa Fluor 488 Conjugated goat anti-mouse IgG, 1:1000, Sant Cruz Biotechnology Inc., USA) for 1 hour at room temperature followed by three times washing with PBS and nuclear staining with HOECHST 33342 (Thermo Fisher, USA).

2.9 Confocal Microscopy

Confocal images were obtained using inverted confocal laser scanning microscope (Olympus Fluoview 1000). Lasers of 488-, 559-, and 633-nm wavelength were used. Objective lenses of 20X and 40X were used to acquire the images with 5µm thickness of each z slice.

2.10 Image Analysis

NIH ImageJ software was used for quantification of confocal images. Percentage MHC positive cells were calculated by taking a ratio of MHC positive cells to the total number of cells in at least 3 images per scaffold type. At least 120 total nuclei were considered per scaffold type. Myotube fusion index was calculated by taking a ratio of number of fused cells containing 2 or more nuclei to total number of cells per image for the Fiber scaffolds. Number of nuclei per myotubes was measured manually and represented as mean ± SD. Myotube maturation index was measured from the immunofluorescence images by calculating ratio of myotubes with 5 or more nuclei to total number of myotubes. The graphs were plotted using Graphpad Prism 6 and Origin Pro 2015.

2.11 Statistics

The results are represented as mean ± standard deviation (n=4-5). The statistical significance between the groups was analyzed using one-way and two-way ANOVA for multiple

comparisons followed by Tukey post-hoc analysis (GraphPad Prism 6). *p* values less than 0.05 were considered statistically significant.

3.0 RESULTS AND DISCUSSION

3.1 CNT and Si-CNT Functionalization Alter Nanoscale Surface Morphology and Wettability of Foam Scaffolds

Cylindrically cut pristine foams or CNT or Si-CNT-functionalized foams (**Figure 1A**) were characterized for their surface morphology (SEM) and wettability (contact angle). **Figure 1B** shows SEM images of pristine (non-functionalized) carbon foams (referred to as Foam hereafter), CNT-coated carbon foam (referred to as CNT-Foam hereafter) and silica-CNT-coated carbon foams (referred to as Si-CNT-Foam hereafter). Carbon foams were coated with either CNTs or further modified with silica (Si-CNT) as described previously [29]. It is evident from **Table 2 and Table 3** that the atomic percentage (At %) of Silica increases from 1.38 to 4.32 which confirms successful nano-functionalization of CNTs with Si. As shown in **Figures B1, B3 and B6**, pristine and functionalized carbon foams exhibited highly interconnected porous structure with similar overall pore size. As shown in **Figure 1 B4** and **B7**, CNT/Si-CNT coating is found to be perpendicular to the surface of Foam scaffolds. Successful CNT/Si-CNT functionalization was further confirmed by high magnification (20,000X) images of the walls of functionalized Foam showing uniform fibrous carpet of CNT/Si-CNT rendering these surfaces nanoscale roughness (**Figure 1 B5, B8**) compared to smooth surface observed for Foam

scaffolds **(Figure 1 B2)**. These SEM images confirm successful coating of CNT carpets on the walls of Foam scaffolds without altering their porosity.

In addition, CNT coating may provide conductive surface to allow better exchange of cellular signals between myoblasts [34]. In addition to the CNT coating, additional layer of silica was applied over CNT carpets coated on foams to modulate contact angle and surface wettability without changing the surface roughness. This allowed decoupling the effects of wettability and nano-roughness on cell adhesion/spreading. Previously Aizenberg group developed revolutionary slippery liquid-infused porous surfaces (SLIPS) by designing nanotextured array of nanoposts functionalized with low-surface energy polyfluoroalkyl silane [35]. This fulfilled a crucial requirement of wetting and facilitating stable adherence of the fluids by providing nano-roughness.

Surface functionalization with nanoscale features is known to alter its hydrophobicity and wettability [35], which can be measured by contact angle of scaffold surface. In a study by Montesano *et al*., atomic force microscopy of PLLA coated with multiwall CNT revealed that increased nano-roughness increased the contact angle and thereby, decreased the surface wetting [36]. Indeed, CNT coating on the Foam surface increased the contact angle from 65-75° to 160° (**Table 1**), making the surfaces more hydrophobic. Hydrophobicity in turn, plays crucial role in interaction of cells with scaffolds, this may become even more important when the scaffolds have macroporous architecture. In these CNT-Foams, nano-scale factors such as nano-roughness and surface wettability are key factors that would influence the cell-scaffold interaction. Therefore, in order to decouple the effects of nano-roughness and wettability on cell adhesion/spreading, CNT-Foams were further functionalized with silica. Silica is an inorganic, bio-resorbable and biocompatible material and have been widely investigated in tissue

engineering, specifically in bone regeneration [37]. Interestingly, silica coating significantly reduced the contact angle of CNT-Foam from 160.3° to 66.5° for Si-CNT-Foam (**Table 1**), which was similar to that of Foam. Thus, Si-CNT-Foam possesses comparable macroporosity, contact angle and wettability to that of Foam with added nano-roughness of CNT-Foam.

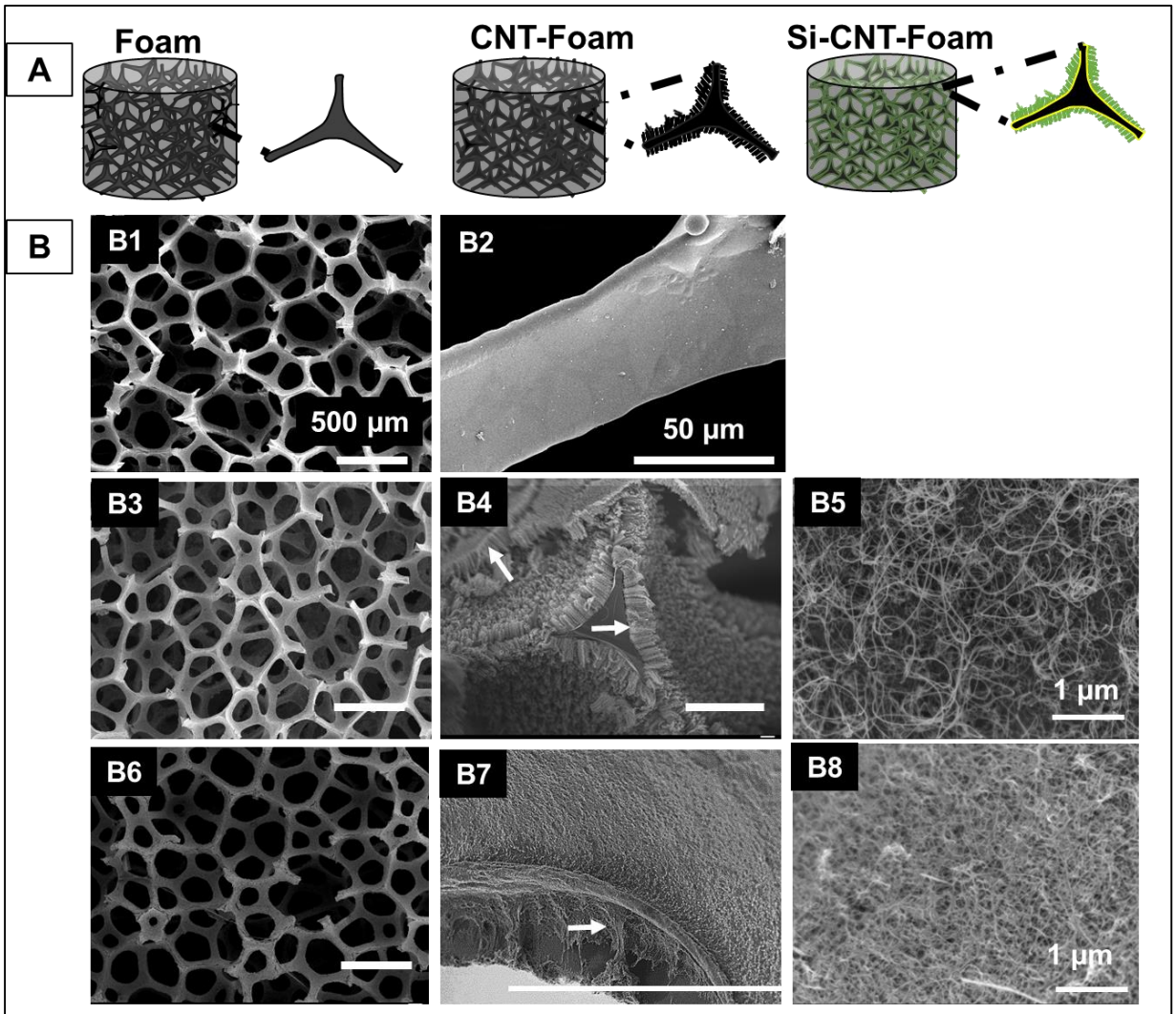

Table 1

Composition	Contact angle (°)
Foam	65-75 °
CNT-Foam	160°
Si-CNT Foam	66.5°

Table 2

Element	At%
CK	95.62
OK	02.81
SiK	01.38
FeK	00.19

Table 3

Element	At%
CK	86.79
OK	07.81
SiK	04.32
FeK	01.08

Figure 1. Functionalization and characterization of carbon foams

A) Schematic of carbon foams functionalized with carbon nanotubes (CNT) and silica-CNT (Si-CNT); B) Effect of surface modification with CNT and Si-CNT on the micro- and nano-structure and surface properties of carbon foams; Low magnification images showing highly interconnected porous structure of pristine Foam (B1), CNT-Foam (B3) and Si-CNT-Foam (B6); High magnification images showing smooth surface of pristine Foams (B2) while CNT (B4) and Si-CNT (B7) coatings conferred nano-roughness (depicted by white arrows), B5: CNT coating and B8: Si-CNT coating at high magnification showing nanofiber structure. Table 1 demonstrates the effect of surface modification on contact angle. Upon CNT coating on the foams, contact angle increased while subsequent coating with Si on CNT-coated foams decreased the contact angle. Table 2 and table 3 show Energy-dispersive X-ray spectroscopy (EDS) analysis of CNT and Si-CNT-coated carbon foams showing atomic percentage of C, O, Si and Fe.

For development of biomaterials, it is critical to understand the role of surface wetting in the attachment of cells on the surface of the biomaterial. Hydrophilic surfaces tend to promote protein adsorption on their surface and mediate cell adhesion directly [38]. Cell adhesion proteins such as fibronectin and laminin further mediate attachment of cells to the biomaterial surface. Contact angle of Foam (**Table 1**) indicated the surface of Foam to be hydrophilic. An *in vitro* study found hydrophilic materials to be more cell-adhesive compared to hydrophobic materials [39]. CNT functionalization increased the contact angle and rendered the surface of CNT-Foam to be hydrophobic. In case of less wettable biomaterial surfaces, cell adhesion proteins get adsorbed and disrupt ordered water molecule, leading to increased entropy, which in turn, acts as a driving force for adhesion. Such entropy-driven adsorption is usually strong and irreversible compared to enthalpy-driven and reversible adsorption on easily wettable surfaces [40]. Extremely hydrophobic surfaces are not desirable for cell activity. Si-CNT Foam showed similar contact angle to Foam which indicated moderately hydrophilic surface. Several studies

have suggested that a moderate range of contact angle around 70° is ideal for cell attachment and spreading [41, 42]. Following the characterization of materials, cell adhesion, spreading, cytocompatibility and their potential for promoting differentiation were assessed.

3.2 Surface Functionalization of Foam Promotes Cell Adhesion, Spreading, Viability and Differentiation of C2C12 Myoblast Cells into Myocytes

In order to test hypothesis that immobilized CNTs will offer cytocompatible surface for myoblast growth and differentiation into myocytes due to various cues (e.g., nano-topography, conductive surfaces and macroporous scaffold architecture) as discussed earlier (**Figure 2A**), we cultured C2C12 cells on Foams. First, the cytocompatibility was assessed by measuring metabolic activity of cells as described in the following section.

3.2.1 Porous Architecture of Foam Allows Cell Infiltration, Adhesion, Spreading and Bioactive Foam Surfaces Promote *De Novo* Matrix Synthesis

Cell infiltration into the Foam scaffold was studied using SEM of the Foams seeded with C2C12 mouse myoblast cells cultured for 21 days. SEM images as shown in **Figure 2 B1, B3 and B5** indicated that cells were able to infiltrate and adhere uniformly in all the 3 Foams. SEM images also showed the spread morphology of cells on the Foams (**Figure 2B2**). Cell adhesion and proliferation on day 1 was further confirmed by metabolic activity assay as shown in **Figure 2F**. In case of Foams (**Figure 2 B1)**, cells appeared as a uniform cell sheet on the surface of the Foam, whereas the presence of nano-hair like CNT increased surface roughness and cells were

attached on to these needle-like projections as shown with white arrows in **Figure 2 B6** (Si-CNT-Foam) and **Figure 2C** (CNT-Foam). Thus, SEM microscopy suggested that CNT array, (**Figure 1 B4 and B7),** was involved in enhancing cell-Foam interactions in functionalized Foams (**Figure 2C)**. *De novo* matrix synthesis is one of the important steps in tissue regeneration on biomaterial scaffolds. Production of functional tissue mimetic structures can be facilitated through biodegradation of scaffolds along with synthesis of new ECM by the seeded cells. In a study reported by Sant *et al.*, Collagen type 1, fibronectin and laminin were secreted by valvular interstitial cells on PGS-PCL scaffolds [43]. In this case, all the 3 conditions, i.e., Foam, CNT-Foam and Si-CNT-Foam facilitated *de novo* ECM secretion, as shown in **Figure 2D**. This confirms that foams themselves are bioactive and their surface functionalization improves bioactivity and facilitates cell adhesion, spreading and *de novo* matrix secretion.

3.2.2 Pristine Foam and Surface-functionalized Foams Exhibit Excellent Cytocompatibility

Cytotoxic effects of CNTs have been studied extensively [44, 45] and reviewed by Hussain *et al.* [46]. CNTs were found to be cytotoxic when they were freely suspended in culture and were available for cellular uptake; however, CNTs immobilized on a matrix or scaffold were found to be non-toxic [46]. Therefore, in this study, CNTs were immobilized as a carpet on foams to mask their cytotoxic effects. The effect of surface modification and wettability on cell adhesion and proliferation of mouse myoblast cells (C2C12) was further investigated by Alamar Blue assay as shown in **Figure 2F**. Alamar Blue assay measures ability of metabolically active cells to reduce resazurin to fluorescent resorufin [47]. All the scaffolds were transferred to new

wells after 24 h, prior to Alamar Blue assay, in order to eliminate the metabolic activity of the cells that were adhered to the plastic but not the scaffolds.

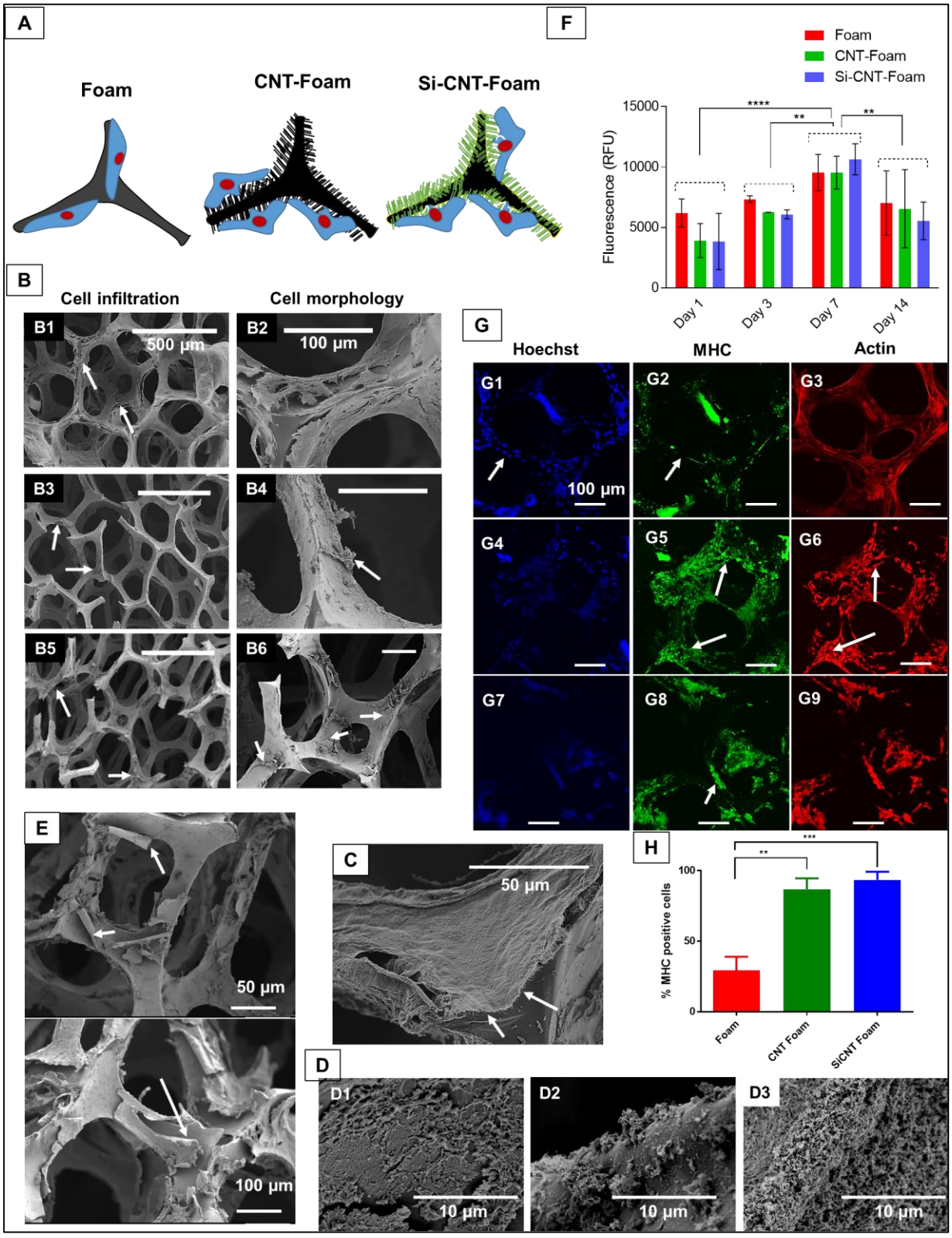

Figure 2. Effect of surface modification on myoblast (C2C12) viability, morphology and differentiation into myocytes

A) C2C12 myoblast cells were seeded onto pristine and functionalized Foams and were allowed to grow 3 days in growth media, followed by differentiation media over a total period of 21 days. B) Scanning electron microscopy images showing cell infiltration throughout the depth of non-functionalized (B1, B2), CNT-Foam (B3, B4), and Si-CNT-Foam (B5, B6). It can be seen that cells adhere to the walls of the pores; white arrows show infiltrated cells. C) Cells interacting with nanoscale needle like CNT projections on the surface of foam as seen in CNT-Foam; white arrows show the interface between CNT and cells. D) *De novo* matrix synthesis in Foam (D1), CNT-Foam (D2) and Si-CNT-Foam (D3); E) Cell sheets peeled off from the walls of Si-CNT Foam along with Si-CNT coating; F) C2C12 cells exhibited time-dependent increase in cell proliferation over a period of first 7 days followed by decrease thereafter, which may be due to onset of their differentiation into myocytes. Statistical significance by two-way ANOVA and Tukey post hoc test. ** denotes $p<0.005$, **** denotes $p<0.00005$; G) Confocal microscopy images showing differentiation of C2C12 cells into myocytes as indicated by myosin heavy chain (MHC) staining. In CNT-Foam (G4, G5, G6) and Si-CNT-Foam (G7, G8, G9) samples, all the cells stained for nuclei and Phalloidin (Actin) also stained positive for MHC. However, multinucleated cellular structures representing myotubes were not observed in any of the scaffolds. White arrows show areas of interest which show differential MHC expression among three types of scaffolds. H) Image analysis showing quantification of percentage MHC-positive cells from n=3 images from differentiation study. Statistical significance by one-way ANOVA and Tukey post hoc test. ** denotes $p<0.005$, *** denotes $p<0.0005$.

All the scaffolds supported growth of C2C12 as evident from the significant increase in their metabolic activity over a period of 7 days. Moreover, statistically non-significant differences between functionalized CNT/Si-CNT-Foam and pristine Foam scaffolds suggested that CNT carpets immobilized onto carbon foams are cytocompatible. We also observed decreased metabolic activity of cells on day 14, which can be attributed to peeling off confluent cell sheets with CNT/Si-CNT carpets from the foam surfaces as shown in representative SEM images for Si-CNT-Foam in **Figure 2E**. This peeling off behavior suggests strong interaction of cells with

underlying CNT/Si-CNT carpets. This may have also prevented cellular uptake of individual CNT, thus improving the cytocompatibity. Another reason for decreased metabolic activity after day 7 could be attributed to myoblasts differentiation to myocytes [48].

3.2.3 CNT Coating Facilitates Differentiation of Myoblasts

It is well known that topographical cues help in guiding differentiation [49]. Thus, we investigated the role of CNT and Si-CNT functionalization on myoblast differentiation. C2C12 cells were cultured on Foams, CNT-Foam and Si-CNT-Foam for 3 days in growth media, followed by another 18 days in differentiation media. The cells were then fixed and stained with Hoechst (nucleus, blue), myosin heavy chain (MHC, green) and phalloidin (actin, red). Consistent with SEM images (**Figure 2 B1-B2**), Foam scaffolds showed C2C12 cells attached and spread on the foam walls as shown by nuclear and cytoskeletal actin staining (**Figure 2 G1 and G3**). However, very few MHC- positive cells were observed (**Figure 2 G2**), indicating their limited ability to differentiate into myocytes. On the contrary, CNT-Foam **(Figure 2 G4-G6)** and Si-CNT-Foam **(Figure 2 G7-G9)** showed presence of much higher number of MHC positive cells, indicating that CNT/Si-CNT functionalization promotes myogenic differentiation. Image analysis confirmed these results revealing significantly higher percentage of MHC-positive cells in CNT-Foam and Si-CNT-Foam as compared to Foam scaffolds (**Figure 2H).** While Foam scaffolds showed only 30% MHC-positive cells, both CNT/Si-CNT-Foams showed significantly higher (about 90%) MHC-positive cells. This may be due to the nano-roughness provided by CNT/Si-CNT as shown in **Figure 1 B5 and B8.** This may also be due to enhanced cell-cell communication as myoblasts need electrically conductive surface for the development of functional muscle tissue and conductive CNT nanosurfaces may enhance transmission of such

signals. In a nutshell, in addition to facilitating cell proliferation, CNT-Foam and Si-CNT-Foam were found to be conducive for myoblast differentiation. This suggests that nano-roughness, which is common to both CNT-Foam and Si-CNT-Foam rather than wettability plays important role in controlling myoblast differentiation into MHC-positive cells. Interestingly, formation of multinucleated myotubes was not evident in any of the three scaffolds. This may be due to the porous geometry of foam scaffolds. Foams provided excellent porosity and surface area that enhanced myoblast cell proliferation and adhesion on all three scaffolds whereas CNT/Si-CNT functionalization provided additional structural cues such as nano-roughness and/or conductivity, which further aided myoblast differentiation into MHC-positive cells. However, foams lack alignment cues, which are present in native skeletal muscle tissue. Although interconnected porous structure along with nanoscale surface functionalization led to myoblast differentiation into MHC-positive cells, it fell short of promoting fusion of these cells into multinucleated myotube-like structures.

3.3 CNT Coating on Woven Aligned Carbon Fibers Affects Surface Morphology and Wettability

Alignment provides instructive pattern for myoblasts during early stages of muscle development [50]. As muscle is a highly organized structure, myotube formation on surfaces with no contact guidance is believed to be immature, for instance, it can form few myoblasts grown in swirled and unorganized pattern [10]. This hampers formation of the myotubes and thereby, the functional regeneration. Aligned structural or topographical cues provide contact

guidance, where myotubes can be formed parallel to each other thereby leading to functional tissue development [5, 51, 52].

In contrast to the porous architecture of foams, fibrous structures mimic the structure of *in vivo* skeletal muscle. We, therefore, developed aligned woven mats of carbon fibers with CNT coating **(Figure 3A)**, which possess multi-scale hierarchy. Woven fiber mats have microscale fibrils forming a horizontal multilayered strip. These strips are then interwoven in similar way to woven cloth fibers as shown in the schematic. Successful CNT-functionalization was confirmed by EDX-SEM elemental analysis **(Table 5). Figure 3B** shows SEM micrographs of pristine carbon fibers (referred to as Fiber hereafter) and CNT-coated carbon fibers (referred to as CNT-Fiber). As shown in **Figure 3 B4,** the overall aligned scaffold architecture at macro-scale remain unchanged after CNT coating while surface roughness was enhanced **(Figure 3 B4-B6)** compared to smooth surface observed for non-functionalized carbon fibers (**Figure 3 B1-B3**)**.** In addition, nanoscale CNTs connecting two parallel carbon fibers were observed as indicated by red arrows in **Figure 3 B6.** CNT coating conferred the nano-roughness to the surface along with interconnected grooves between parallel fibers without compromising fiber alignment. CNT coating also increased contact angle of the scaffolds similar to CNT-Foam as shown in **Figure 3 C** and **Table 4.**

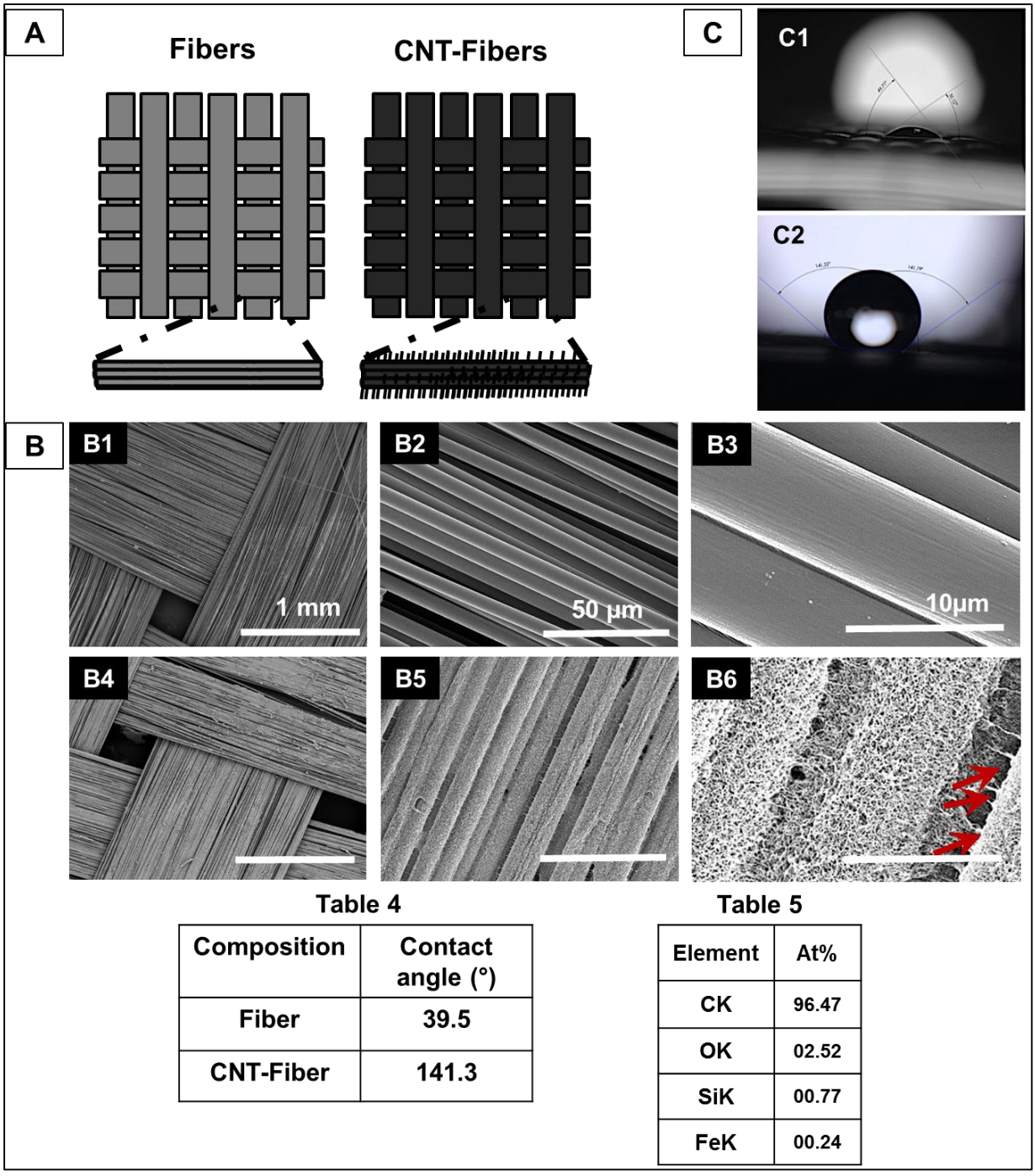

Table 4

Composition	Contact angle (°)
Fiber	39.5
CNT-Fiber	141.3

Table 5

Element	At%
CK	96.47
OK	02.52
SiK	00.77
FeK	00.24

Figure 3. Functionalization and characterization of aligned carbon fiber scaffolds

A) Aligned carbon fiber mats were functionalized with CNT (CNT-Fibers). B) Scanning electron microscopy images showing increased surface roughness after CNT functionalization (B4-B6) in contrast to smooth surface of non-functionalized carbon fibers (B1-B3). C) CNT functionalization increased contact angle and thus, hydrophobicity of the CNT-Fiber scaffolds as indicated in Table 4. As evident from the study of Si-CNT functionalized foam, wettability did not show any significant effect on myoblast differentiation, therefore Silica functionalization was not considered in similar study with fibers.

3.4 Effect of Surface Modification of Woven Fibers on Attachment and Proliferation of C2C12 Mouse Myoblast Cells

C2C12 myoblast cells were seeded on pristine (Fiber) and functionalized CNT-Fiber scaffolds (**Figure 4A**) to mainly elucidate the effect of fiber alignment coupled with CNT functionalization on cellular proliferation, alignment and differentiation.

Several studies suggest that myoblast differentiation is enhanced in aligned fibrous scaffold compared to randomly oriented ones [19, 53-55]. Metabolic activity of seeded cells was evaluated for 14 days using Alamar Blue assay **(Figure 4B)**. Fiber scaffolds showed increased metabolic activity throughout 14 days while CNT-fiber showed significantly higher metabolic activity until day 3 compared to carbon fibers ($p<0.05$), after which CNT-Fiber reached confluence and no significant change was observed for next 14 days. This may be attributed to stimulation of myogenic differentiation by CNT coating. While Fiber scaffolds showed cell adhesion/spreading and facilitated formation of multicellular structures (black arrow in **Figure 4C2)**, randomly orientated and less organized cell aggregates can also be observed. On the other

hand, CNT-Fiber promoted aligned multicellular structures completely covering entire area of the CNT-Fiber scaffold (almost 2.5 mm) as shown in **Figure 4, C4 and C5)**. CNT-Fiber scaffolds also promoted cell-material interaction to achieve great contact adhesion as indicated by white arrows (cell bodies) and red arrows (CNTs) (**Figure 4 C6**).

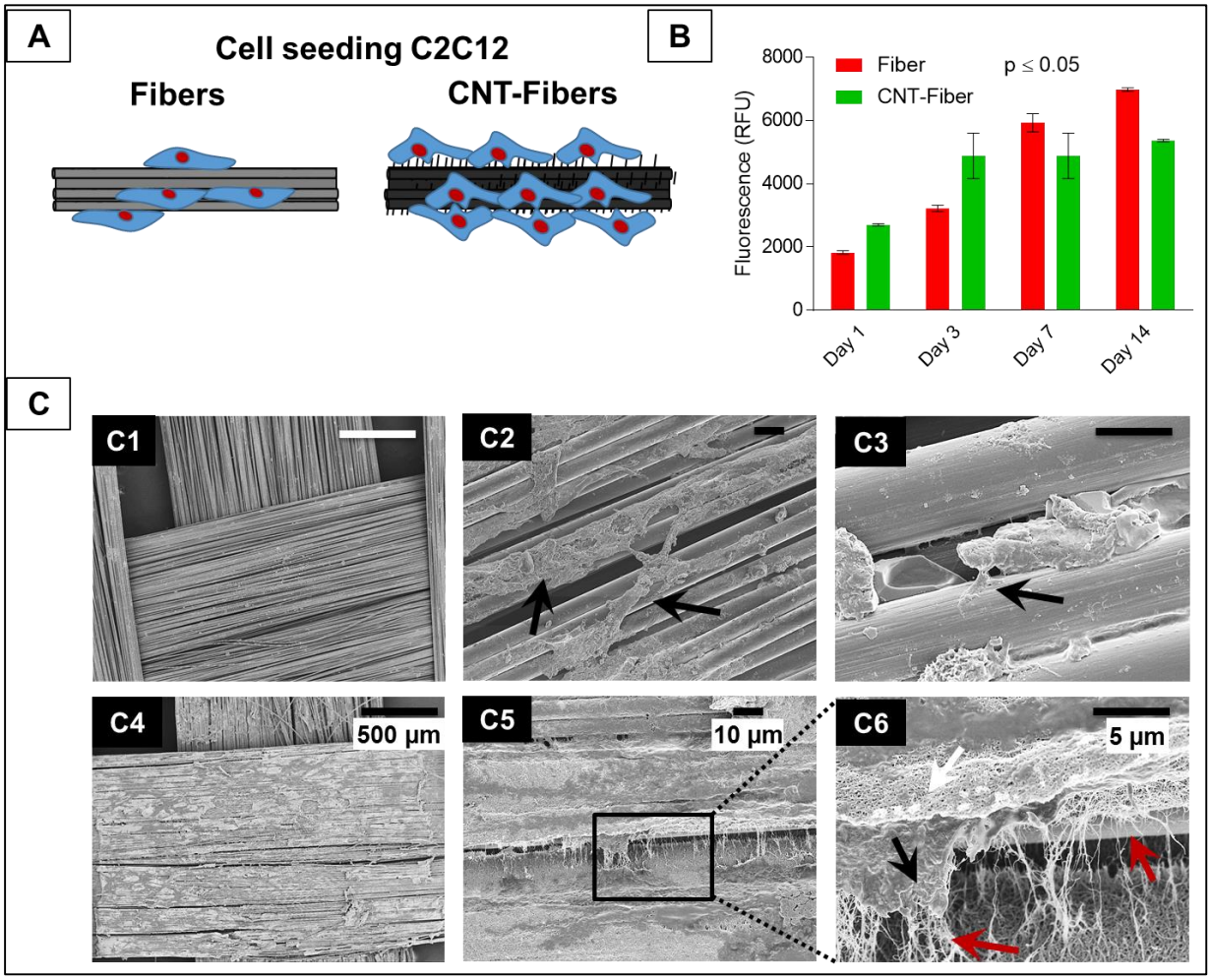

Figure 4. Effect of CNT functionalization of aligned carbon fibers on attachment and proliferation of C2C12 mouse myoblast cells

A) C2C12 myoblast cells were seeded on Fiber and CNT- Fiber scaffolds. B) C2C12 proliferation on Fiber and CNT- Fiber scaffolds. Statistically significant difference was found amongst all groups ($p < 0.05$) by two-way ANOVA and Tukey post-hoc test. C) Scanning electron microscopy images showing C2C12 interaction with the underlying Fiber and CNT- Fiber samples. Significantly increased number of cells can be observed on the CNT-Fiber samples with cell bodies (black arrows) interacting with the CNTs (red arrows) coated on carbon fibers.

3.5 Aligned Fibrous Structure along with CNT Functionalization Facilitate Differentiation of Myoblast Cells into Continuous Myotubes

We further investigated the collective influence of fiber alignment and nano-roughness of Fiber and CNT-Fiber scaffolds on differentiation of C2C12 myoblast cells over 14 days (Schematic in **Figure 5A).** We selected earlier time point of 14 days in Fiber scaffolds as most of the confluent cellular structures formed during 21 days were detached from the scaffolds preventing any analysis of MHC-positive cells (data not shown). This suggested that aligned fibrous scaffolds may be more efficient in promoting differentiation at earlier time point. Indeed, low magnification confocal microscopy images of MHC (green) and nuclei showed MHC-positive cells in both Fiber (pristine) and CNT-Fiber scaffolds unlike foam scaffolds. While Fiber scaffolds showed MHC-positive multinucleated cells scattered throughout the image area (Figure 5B, top panel), CNT-Fiber scaffolds showed interconnected, multinucleated MHC-positive cells covering entire area of the image, suggesting efficient fusion of differentiated

myocytes to form myotubes (**Figure 5B)**. Higher magnification images in **Figure 5C** showed aligned myotubes parallel to fiber direction.

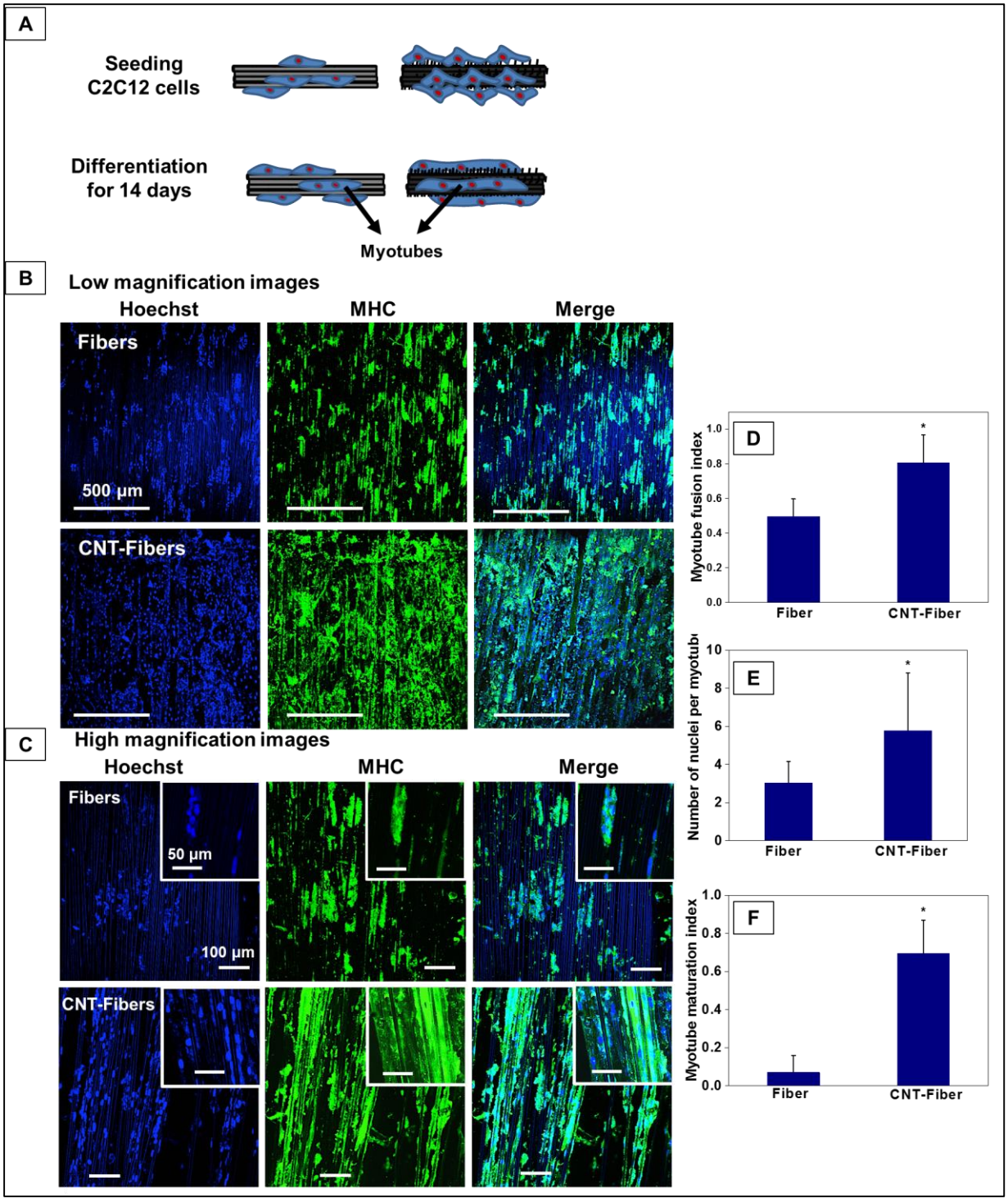

Figure 5. Effect of fiber alignment on C2C12 mouse myoblast differentiation

A) C2C12 myoblast cells were cultured on pristine fibers and CNT fibers and were allowed to differentiate for 14 days. B) Low magnification confocal microscopy images showed differentiation of C2C12 cells into myocytes as indicated by myosin heavy chain (MHC) staining. In CNT-Fiber, all the cells stained for MHC (green). Nuclei were stained with Hoechst (blue). Interestingly, CNT-Fibers showed continuous multinucleated cell structures spread across the entire scaffold surface. C) High magnification confocal microscopy images showing differentiation of C2C12 cells into myocytes and formation of continuous multinucleated myotubes indicated by MHC and nuclear staining. Very high magnification images (insets in bottom panel) showed formation of continuous myotubes forming structures similar to muscle fiber bundles. D) Myotube fusion index (Cells containing 2 or more nuclei/ total number of cells per image). E) Number of nuclei per myotube. F) Myotube maturation index (ratio of myotubes with 5 or more nuclei to total number of myotubes). In both the cases, CNT-Fiber shows increased fusion and maturation indices compared to pristine carbon Fiber, * shows significant difference at $p<0.05$ compared to carbon Fibers; statistical analysis was done using student t-test.

Most interestingly, CNT-Fiber showed formation of myotube fiber bundles which are believed to be units of functional muscle tissue. Further image analysis revealed significantly higher myotube fusion index in CNT-Fibers compared to carbon fibers (**Figure 5D**). Similarly, number of nuclei per myotube and myotube maturation index (myotubes containing more than 5 nuclei) were found to be significantly higher in CNT-Fiber scaffolds compared to Fiber scaffolds. As discussed under **section 3.5**, functionalized Foams showed significantly higher MHC-positive cells (**Figure 2H**), however, they failed to stimulate fusion of differentiated myocytes unlike CNT-fiber which show fusion of myocytes into multinucleated myotubes. These results strongly suggest an important role played by the aligned fibrous architecture. It has been reported that end to end fusion of myocytes or myoblasts is more feasible than lateral fusion, therefore, oriented cells due to alignment cues are more likely to undergo such fusion [51,

56]. Moreover, other studies have revealed that narrow width of aligned structures promoted densely packed myotubes resembling functional myotubes [52, 57]. This supports our observations of improved myotube fusion in even Fiber scaffolds, which possess fibers with around 10 micron diameter.

4.0 CONCLUSION AND FUTURE DIRECTION

In this study, carbon-based material was common base material throughout all scaffolds. By comparing Foam (pristine) and Fiber (pristine) scaffolds, it is evident that the scaffold architecture (interconnected porous *vs* aligned fibrous structure) played an important role for facilitating fusion of myocytes to form multinucleated myotubes. Pristine Foam scaffolds showed few MHC positive myocytes, however, fused and continuous myotubes were not found, whereas pristine Fiber scaffolds promoted fusion of differentiated myocytes into multinucleated myotubes. CNT-functionalization was found to enhance myoblast differentiation into myocytes in both the foam and fiber scaffolds. CNT-foam or Si-CNT foam did not promote fusion of myocytes into multinucleated myotubes even though they enhanced MHC positive cells in comparison with Foam scaffolds. This also suggested minimal effect of contact angle on cell differentiation. More interestingly, CNT-Fiber scaffolds were found to be the most suitable material which can facilitate formation of multinucleated myotubes. This was mainly due to excellent contact guidance provided by aligned fibrous architecture along with nano-roughness and conductive surface. End to end fusion of myotubes was facilitated due to the combined influence of above-mentioned factors. In conclusion, CNT-functionalized carbon fibers have potential for skeletal muscle repair and regeneration.

Future studies will involve exploring differential expression of genes involved in myogenesis. This will provide mechanistic understanding of how different scaffold architecture

and CNT nano-functionalization affect myogenesis. It is worthwhile to carryout animal studies by implanting pre-seeded scaffolds with progenitor cells derived from the same animals as well as non-cell seeded scaffolds and assessing regeneration of functional muscle tissue.

APPENDIX A

ABBREVIATIONS

Term	Abbreviation
ECM	Extracellular Matrix
SEM	Scanning Electron Microscopy
CNT	Carbon Nanotube
Si	Silica
MHC	Myosin Heavy Chain

BIBLIOGRAPHY

[1] Vilquin JT. Myoblast transplantation: Clinical trials and perspectives. Mini-review. Acta Myologica. 2005;24:119-27.

[2] Bach AD, Beier JP, Stern-Staeter J, Horch RE. Skeletal muscle tissue engineering. Journal of Cellular and Molecular Medicine. 2004;8:413-22.

[3] Osses N, Brandan E. ECM is required for skeletal muscle differentiation independently of muscle regulatory factor expression. Am J Physiol Cell Physiol. 2002;282:C383-94.

[4] Hinds S, Bian W, Dennis RG, Bursac N. The role of extracellular matrix composition in structure and function of bioengineered skeletal muscle. Biomaterials. 2011;32:3575-83.

[5] Lam MT, Huang Y-C, Birla RK, Takayama S. Microfeature guided skeletal muscle tissue engineering for highly organized 3-dimensional free-standing constructs. Biomaterials. 2009;30:1150-5.

[6] Sant S, Coutinho DF, Sadr N, Reis RL, Khademhosseini A. Tissue Analogs by the Assembly of Engineered Hydrogel Blocks. Biomimetic Approaches for Biomaterials Development: Wiley-VCH Verlag GmbH & Co. KGaA; 2012. p. 471-93.

[7] Bae H, Chu H, Edalat F, Cha JM, Sant S, Kashyap A, et al. Development of functional biomaterials with micro- and nanoscale technologies for tissue engineering and drug delivery applications. Journal of Tissue Engineering and Regenerative Medicine. 2014;8:1-14.

[8] Fedorovich NE, Alblas J, de Wijn JR, Hennink WE, Verbout AJ, Dhert WJ. Hydrogels as extracellular matrices for skeletal tissue engineering: state-of-the-art and novel application in organ printing. Tissue engineering. 2007;13:1905-25.

[9] Rossi CA, Flaibani M, Blaauw B, Pozzobon M, Figallo E, Reggiani C, et al. In vivo tissue engineering of functional skeletal muscle by freshly isolated satellite cells embedded in a photopolymerizable hydrogel. The FASEB Journal. 2011;25:2296-304.

[10] Riboldi SA, Sampaolesi M, Neuenschwander P, Cossu G, Mantero S. Electrospun degradable polyesterurethane membranes: potential scaffolds for skeletal muscle tissue engineering. Biomaterials. 2005;26:4606-15.

[11] Place ES, Evans ND, Stevens MM. Complexity in biomaterials for tissue engineering. Nature materials. 2009;8:457-70.

[12] Schoen FJ, Mitchell RN. Chapter II.1.5 - Tissues, the Extracellular Matrix, and Cell–Biomaterial Interactions. In: Lemons BDRSHJSE, editor. Biomaterials Science (Third Edition): Academic Press; 2013. p. 452-74.

[13] Parker KK, Ingber DE. Extracellular matrix, mechanotransduction and structural hierarchies in heart tissue engineering. Philosophical Transactions of the Royal Society B: Biological Sciences. 2007;362:1267-79.

[14] El-Ayoubi R, Eliopoulos N, Diraddo R, Galipeau J, Yousefi A-M. Design and fabrication of 3D porous scaffolds to facilitate cell-based gene therapy. Tissue Eng Part A. 2008;14:1037-48.

[15] Engelmayr GC, Cheng M, Bettinger CJ, Borenstein JT, Langer R, Freed LE. Accordion-like honeycombs for tissue engineering of cardiac anisotropy. Nature materials. 2008;7:1003-10.

[16] Park H, Larson BL, Guillemette MD, Jain SR, Hua C, Engelmayr Jr GC, et al. The significance of pore microarchitecture in a multi-layered elastomeric scaffold for contractile cardiac muscle constructs. Biomaterials. 2011;32:1856-64.

[17] Nuttelman CR, Mortisen DJ, Henry SM, Anseth KS. Attachment of fibronectin to poly(vinyl alcohol) hydrogels promotes NIH3T3 cell adhesion, proliferation, and migration. Journal of Biomedical Materials Research. 2001;57:217-23.

[18] Ahadian S, Ramon-Azcon J, Estili M, Liang X, Ostrovidov S, Shiku H, et al. Hybrid hydrogels containing vertically aligned carbon nanotubes with anisotropic electrical conductivity for muscle myofiber fabrication. Sci Rep. 2014;4:4271.

[19] Chen M-C, Sun Y-C, Chen Y-H. Electrically conductive nanofibers with highly oriented structures and their potential application in skeletal muscle tissue engineering. Acta Biomaterialia. 2013;9:5562-72.

[20] He Y, Chen W, Gao C, Zhou J, Li X, Xie E. An overview of carbon materials for flexible electrochemical capacitors. Nanoscale. 2013;5:8799-820.

[21] Lu Y, Huang Y, Zhang M, Chen Y. Nitrogen-doped graphene materials for supercapacitor applications. J Nanosci Nanotechnol. 2014;14:1134-44.

[22] Wang H, Yuan X, Zeng G, Wu Y, Liu Y, Jiang Q, et al. Three dimensional graphene based materials: Synthesis and applications from energy storage and conversion to electrochemical sensor and environmental remediation. Adv Colloid Interface Sci. 2015.

[23] Czarnecki JS, Jolivet S, Blackmore ME, Lafdi K, Tsonis PA. Cellular automata simulation of osteoblast growth on microfibrous-carbon-based scaffolds. Tissue Eng Part A. 2014;20:3176-88.

[24] Depan D, Misra RDK. The development, characterization, and cellular response of a novel electroactive nanostructured composite for electrical stimulation of neural cells. Biomaterials Science. 2014;2:1727-39.

[25] Chen J, Chen S, Zhao X, Kuznetsova LV, Wong SS, Ojima I. Functionalized Single-Walled Carbon Nanotubes as Rationally Designed Vehicles for Tumor-Targeted Drug Delivery. Journal of the American Chemical Society. 2008;130:16778-85.

[26] Lacerda L, Bianco A, Prato M, Kostarelos K. Carbon nanotubes as nanomedicines: From toxicology to pharmacology. Advanced Drug Delivery Reviews. 2006;58:1460-70.

[27] Harrison BS, Atala A. Carbon nanotube applications for tissue engineering. Biomaterials. 2007;28:344-53.

[28] Li N, Zhang Q, Gao S, Song Q, Huang R, Wang L, et al. Three-dimensional graphene foam as a biocompatible and conductive scaffold for neural stem cells. Sci Rep. 2013;3.

[29] Karumuri AK, He L, Mukhopadhyay SM. Tuning the surface wettability of carbon nanotube carpets in multiscale hierarchical solids. Applied Surface Science. 2015;327:122-30.

[30] McKeon-Fischer K, Flagg D, Freeman J. Coaxial electrospun poly (ε-caprolactone), multiwalled carbon nanotubes, and polyacrylic acid/polyvinyl alcohol scaffold for skeletal muscle tissue engineering. Journal of Biomedical Materials Research Part A. 2011;99:493-9.

[31] Spinks GM, Mottaghitalab V, Bahrami-Samani M, Whitten PG, Wallace GG. Carbon-Nanotube-Reinforced Polyaniline Fibers for High-Strength Artificial Muscles. Advanced Materials. 2006;18:637-40.

[32] Sharmila MM, Anil K, Ian TB. Hierarchical nanostructures by nanotube grafting on porous cellular surfaces. Journal of Physics D: Applied Physics. 2009;42:195503.

[33] Sharmila MM, Anil KK. Nanotube attachment for prevention of interfacial delamination. Journal of Physics D: Applied Physics. 2010;43:365301.

[34] Shin SR, Jung SM, Zalabany M, Kim K, Zorlutuna P, Kim Sb, et al. Carbon-Nanotube-Embedded Hydrogel Sheets for Engineering Cardiac Constructs and Bioactuators. ACS Nano. 2013;7:2369-80.

[35] Wong T-S, Kang SH, Tang SKY, Smythe EJ, Hatton BD, Grinthal A, et al. Bioinspired self-repairing slippery surfaces with pressure-stable omniphobicity. Nature. 2011;477:443-7.

[36] Montesano S, Lizundia E, D'Angelo F, Fortunati E, Mattioli S, Morena F, et al. Nanocomposites Based on PLLA and Multi Walled Carbon Nanotubes Support the Myogenic Differentiation of Murine Myoblast Cell Line. ISRN Tissue Engineering. 2013;2013.

[37] Gaharwar AK, Mihaila SM, Swami A, Patel A, Sant S, Reis RL, et al. Bioactive silicate nanoplatelets for osteogenic differentiation of human mesenchymal stem cells. Adv Mater. 2013;25:3329-36.

[38] Ferlin KM, Kaplan DS, Fisher JP. Characterization of the Adhesive Interactions Between Cells and Biomaterials. Micro and Nanotechnologies in Engineering Stem Cells and Tissues: John Wiley & Sons, Inc.; 2013. p. 159-82.

[39] Schakenraad JM, Busscher HJ, Wildevuur CR, Arends J. The influence of substratum surface free energy on growth and spreading of human fibroblasts in the presence and absence of serum proteins. J Biomed Mater Res. 1986;20:773-84.

[40] JA C. Biomaterials: Protein–surface interactions. In: JD B, editor. biomedical engineering handbook: CRC Press, Inc.-IEEE Press; 1995. p. 1597–608.

[41] Tamada Y, Ikada Y. Effect of Preadsorbed Proteins on Cell Adhesion to Polymer Surfaces. Journal of Colloid and Interface Science. 1993;155:334-9.

[42] Nuttelman CR, Mortisen DJ, Henry SM, Anseth KS. Attachment of fibronectin to poly(vinyl alcohol) hydrogels promotes NIH3T3 cell adhesion, proliferation, and migration. J Biomed Mater Res. 2001;57:217-23.

[43] Sant S, Iyer D, Gaharwar AK, Patel A, Khademhosseini A. Effect of biodegradation and de novo matrix synthesis on the mechanical properties of valvular interstitial cell-seeded polyglycerol sebacate–polycaprolactone scaffolds. Acta Biomaterialia. 2013;9:5963-73.

[44] Yang H, Liu C, Yang D, Zhang H, Xi Z. Comparative study of cytotoxicity, oxidative stress and genotoxicity induced by four typical nanomaterials: the role of particle size, shape and composition. Journal of applied Toxicology. 2009;29:69-78.

[45] Zhang Y, Ali SF, Dervishi E, Xu Y, Li Z, Casciano D, et al. Cytotoxicity Effects of Graphene and Single-Wall Carbon Nanotubes in Neural Phaeochromocytoma-Derived PC12 Cells. ACS Nano. 2010;4:3181-6.

[46] Hussain MA, Kabir MA, Sood AK. On the cytotoxicity of carbon nanotubes. Current Science. 2009;96:664-73.

[47] Mukundan S, Sant V, Goenka S, Franks J, Rohan LC, Sant S. Nanofibrous composite scaffolds of poly(ester amides) with tunable physicochemical and degradation properties. European Polymer Journal. 2015;68:21-35.

[48] Sirivisoot S, Harrison BS. Skeletal myotube formation enhanced by electrospun polyurethane carbon nanotube scaffolds. International journal of nanomedicine. 2011;6:2483.

[49] Kerativitayanan P, Carrow JK, Gaharwar AK. Nanomaterials for Engineering Stem Cell Responses. Advanced Healthcare Materials. 2015:n/a-n/a.

[50] Choi JS, Lee SJ, Christ GJ, Atala A, Yoo JJ. The influence of electrospun aligned poly (ε-caprolactone)/collagen nanofiber meshes on the formation of self-aligned skeletal muscle myotubes. Biomaterials. 2008;29:2899-906.

[51] Clark P, Coles D, Peckham M. Preferential Adhesion to and Survival on Patterned Laminin Organizes Myogenesisin Vitro. Experimental Cell Research. 1997;230:275-83.

[52] Evans DJR, Britland S, Wigmore PM. Differential response of fetal and neonatal myoblasts to topographical guidance cues in vitro. Dev Gene Evol. 1999;209:438-42.

[53] Ku SH, Lee SH, Park CB. Synergic effects of nanofiber alignment and electroactivity on myoblast differentiation. Biomaterials. 2012;33:6098-104.

[54] Aviss K, Gough J, Downes S. Aligned electrospun polymer fibres for skeletal muscle regeneration. Eur Cell Mater. 2010;19:193-204.

[55] Riboldi S, Sadr N, Pigini L, Neuenschwander P, Simonet M, Mognol P, et al. Skeletal myogenesis on highly orientated microfibrous polyesterurethane scaffolds. Journal of Biomedical Materials Research Part A. 2008;84:1094-101.

[56] Clark P, Dunn GA, Knibbs A, Peckham M. Alignment of myoblasts on ultrafine gratings inhibits fusion in vitro. The International Journal of Biochemistry & Cell Biology. 2002;34:816-25.

[57] Duffy RM, Feinberg AW. Engineered skeletal muscle tissue for soft robotics: fabrication strategies, current applications, and future challenges. Wiley Interdisciplinary Reviews: Nanomedicine and Nanobiotechnology. 2014;6:178-95.